ICHEP'96 Ref. pa07-043
Submitted to Pa 07, Pa 10
Pa 12, Pa 13
Pl 09, Pl 12

DELPHI 96-80 CONF 12
25 June, 1996

A study of the reaction $e^+e^- \to \mu^+\mu^-\gamma_{isr}$ at LEP and search for new physics near $\sqrt{s} = 80$ GeV

DELPHI Collaboration

ICHEP'96 Ref. pa07-043
Submitted to Pa 7, 10, 12, 13
Pl 9, 12

DELPHI 96-80 CONF 12
25 June, 1996

A study of the reaction $e^+e^- \to \mu^+\mu^-\gamma_{isr}$ at LEP and search for new physics near $\sqrt{s} = 80$ GeV

Preliminary

DELPHI Collaboration

F. Cao, C. De Clercq and J. Lemonne

Abstract

The work presented in this paper has been carried out using data collected by the DELPHI experiment from 1991 to 1994. An analysis is reported on the channel $e^+e^- \to \mu^+\mu^-\gamma_{isr}$. The data are used to extract the total cross section below the Z^0 peak by using the events with relatively hard initial state radiative photon(s) ($E_\gamma > 1$ GeV). The differential cross section as a function of the muon polar production angle is also determined to extract the forward-backward asymmetries for the reaction $e^+e^- \to \mu^+\mu^-$ at energies between 20 and 87 GeV. The ratio of the helicity cross sections $\frac{\sigma_{LL}+\sigma_{RR}}{\sigma_{RL}+\sigma_{LR}}$, with i(j) in σ_{ij} the polarisation of the incoming e^- (outgoing μ^-) fermion, is extracted from the differential cross sections with the aim of testing the Standard Model and to look for new physics near 80 GeV.

1 Introduction

In this paper experimental results from studies of events collected in the channel $e^+e^- \to \mu^+\mu^-\gamma_{isr}$, with γ_{isr} being an initial state radiation photon, at LEP are used to probe the cross sections and asymmetries in the energy region between LEP and TRISTAN and down to PETRA energies. Also an analysis is performed in terms of helicity cross sections to look for new physics near $\sqrt{s} = 80$GeV.

The investigation of the $e^+e^- \to \mu^+\mu^-$ cross section at energies below the Z^0 peak is attractive because no experiments have ever taken data at energies between 61 and 88 GeV. In addition, results from TRISTAN [1] could indicate a deviation of the cross section from the predictions of the Standard Model (SM) at 58 GeV. Measurable deviations in the $e^+e^- \to f\bar{f}$ cross section in this energy range are predicted by several models beyond the SM, for instance those which introduce an additional Z' gauge boson.

In a previous paper [2] an analysis was presented of radiative muon events using the data collected by DELPHI up to 1992. In this paper a new analysis is presented based on the data collected between 1991 and 1994, and on an improved event selection procedure.

The paper is organised as follows. Section 2 summarises the theoretical background to the analysis. Section 3 describes briefly the DELPHI detector and presents the data samples used. In section 4 the event selection procedures are discussed. In section 5 the calculation of the cross sections is presented while the analysis of the differential cross sections in terms of the asymmetry and the helicity cross sections is presented in section 6. The summary is presented in Section 7.

2 Theoretical background

2.1 Total cross section

Electromagnetic radiative corrections to the interaction $e^+e^- \to f\bar{f}$ distort substantially the Born-level cross section at energies around the Z^0 pole ([3], [4]).

Most of the effects can be understood to arise from initial state radiation (ISR), after which the effective annihilation energy of the e^+e^- system is less than the total centre of mass energy $\sqrt{s}$. Because the Born cross section varies rapidly across the Z^0 pole, the resulting changes in the cross section are large and need to be understood very precisely in order to study the underlying electroweak physics.

The cross section for $e^+e^- \to \mu^+\mu^-$ has contributions from direct Z^0 and photon terms and $\gamma - Z^0$ interference. Radiative corrections can be conveniently divided into the following components:

- Emission of real photons from the incident and/or final state fermions.
- Corrections to the Z^0 and γ propagators. These consist of loop diagrams involving any particles which couple to these bosons.
- Vertex corrections. These involve virtual photons as well as any other particles which couple to the initial or final fermions.
- Box diagrams, involving the exchange of two bosons (γ, Z^0).

At the present level of precision, the box diagrams can be neglected. The effect of the vertex and propagator corrections can, to a very good approximation, be absorbed in a redefinition of the Born-level parameters, such that the structure of the Born-level formulae is retained (Improved or Effective Born Approximation; e.g. [4]).

Pure QED initial state corrections can be described by a radiator function $H_i(s,s')$, giving the probability density of emitting a photon with a fraction of the beam energy from the initial state, such that the observed cross section for $e^+e^- \to f\bar{f}$ can be written:

$$\sigma_{obs}^{f\bar{f}}(s) = \int_{s_0'}^{s} \sigma_W^{f\bar{f}}(s') H_i(s,s') ds' \tag{1}$$

where

$$4m_f^2 = s_0' \leq s' \leq s.$$

The invariant mass $M_{\mu\mu}$ of the produced fermion pair is given by $\sqrt{s'}$. In equation (1) $\sigma_W^{f\bar{f}}(s')$ is the Improved Born cross section.

It can be seen from equation (1) that the observed cross section involves a convolution of $\sigma_W^{f\bar{f}}(s')$ with the radiator function H_i. A similar formula can be written for the case when selection criteria are applied to the final state fermions or the photons produced. In addition, there is a small initial-final state radiation interference contribution to the cross section [5]. This interference is very small in the energy region covered by this analysis, $s' < 87GeV$ and $E_\gamma > 1GeV$, and can be neglected at the present level of precision. For the case that a pure ISR sample is selected, the number of events in a given interval $(s', s'+ds')$ can be written as

$$dN = LH_i(s,s')\sigma_W^{f\bar{f}}(s')ds' \tag{2}$$

where L is the integrated luminosity.

As $H_i(s,s')$ is a well known function in QED, with knowledge of the integrated luminosity one can determine the Improved Born cross section below the nominal LEP energies by measuring the $\sqrt{s'}$ spectrum from the invariant mass of the final state dimuon pairs.

2.2 New physics near the zeroes of the $e^+e^- \to \mu^+\mu^-$ cross section

At tree level the $e^+e^- \to \mu^+\mu^-$ cross section can be written, apart from radiative corrections and possible new physics, as

$$\sigma = \sigma_{LL} + \sigma_{RR} + \sigma_{RL} + \sigma_{LR} \tag{3}$$

where i(j) in σ_{ij} stands for the polarisation of the incoming e^- (outgoing μ^-) [6]. Within the Standard Model, σ_{LL} and σ_{RR} have closeby zeroes such that $(\sigma_{LL} + \sigma_{RR})$ nearly vanishes near $\sqrt{s} = 80$ GeV. This is not the case for $(\sigma_{RL} + \sigma_{LR})$, which vanishes at $\sqrt{s} > m_Z$. A study of the cross section sum $\sigma_{LL} + \sigma_{RR}$ around 80 GeV, allows a search for new physics in an environment of minimal background.

As shown in reference [6], due to their angular dependence of the form $(1 \pm \cos\theta)^2$, the two helicity components of the cross section $\sigma_{LL} + \sigma_{RR}$ and $\sigma_{RL} + \sigma_{LR}$, can be extracted

from the data by a polynomial projection of the differential cross section as function of the muon polar production angle:

$$\tilde{\sigma}^{\mu}_{+} = \int_{-C_M}^{C_M} \frac{d\sigma}{dcos\theta}.F_{+}.dcos\theta \tag{4}$$

$$\tilde{\sigma}^{\mu}_{-} = \int_{-C_M}^{C_M} \frac{d\sigma}{dcos\theta}.F_{-}.dcos\theta \tag{5}$$

The filters $F_{\pm}$ are polynomials of the form $A(1 \pm Bcos\theta)$ and $C_M = cos\theta_{max}$ represents the limits in analysis acceptance.

In the framework of the Standard Model

$$\tilde{\sigma}^{\mu}_{+} = \sigma_{LL} + \sigma_{RR} + rad.corr. \tag{6}$$

$$\tilde{\sigma}^{\mu}_{-} = \sigma_{LR} + \sigma_{RL} + rad.corr. \tag{7}$$

and the ratio

$$\frac{\tilde{\sigma}^{\mu}_{+}}{\tilde{\sigma}^{\mu}_{-}} = \frac{\sigma_{LL} + \sigma_{RR}}{\sigma_{RL} + \sigma_{LR}} \tag{8}$$

has a minimum just below 80 GeV. Therefore, this ratio is very sensitive to new physics near this energy. In equation (8), initial and final state soft radiation can be expected to factorize so that the ratio would not be significantly affected. The other radiative corrections are small.

3 The DELPHI detector

The DELPHI detector is described in detail in [7]. In this analysis tracking was performed by the Vertex Detector(VD), the Inner Detector(ID), the Outer Detector(OD), the Time Projection Chamber(TPC) and the Forward Chambers(FCA,FCB). In the rejection of events with final state radiation (FSR) the barrel and forward electromagnetic calorimeters were used (HPC and FEMC). The identification of muons was based on the muon chambers(MUB,MUF), the hadron calorimeter (HCAL) and the electromagnetic calorimeters. In what follows the barrel region was defined as $43^{\circ} \leq \theta \leq 137^{\circ}$, and the endcaps as $\theta < 43^{\circ}$ and $\theta > 137^{\circ}$, where θ is the polar angle with respect to the beam.

The data used for the calculation of the asymmetries and the helicity cross section ratios were collected during the years 1991 to 1994, and correspond to an integrated luminosity of around 115pb^{-1}. For the calculation of the cross sections the data taken during the years 1992-1994 were used, and correspond to an integrated luminosity of around 100 pb^{-1}.

For simulation studies dimuon events were generated using the DYMU3 [8] program. The events were generated with up to two initial state photons and at most one final state photon. For the cross section studies, where a normalisation to the Monte Carlo sample is needed, a total of 613K events were generated, spread over the beam energies at which data were taken in the period 1992-1994. For the evaluation of the efficiency and purity of the ISR sample (see 4.3) 240K radiative muon events with invariant mass $M_{\mu\mu} < 88\text{GeV/c}^2$ were generated at the same beam energies.

For the study of the background from the channel $e^+e^- \rightarrow \tau^+\tau^-$ 270K events were generated with the KORALZ [9] program.

For the study of the background coming from $\gamma\gamma$ processes, 236K $e^+e^- \to e^+e^-\mu^+\mu^-$ and 10K $e^+e^- \to e^+e^-\tau^+\tau^-$ events were generated using the FERMISV program [10].

All generated events were passed through the full DELPHI simulation and the same data reconstruction program as the real data.

4 Selection of dimuon events with Initial State Radiation

The selection of dimuon events with ISR was performed in two steps. First a sample of dimuon events with or without photon production was selected following the procedure discussed in 4.1. From this sample the events with ISR were extracted using the procedure detailed in 4.2.

For the calculation of the cross sections the same selection procedure was applied to the 613K simulated dimuon events (see section 3).

4.1 Selection of $e^+e^- \to \mu^+\mu^-(n\gamma)$ events

To select a sample of dimuon events allowing for possible photon emission the same procedure was followed as explained in [11] with some modifications to allow for a larger fraction of radiative events, and with a more elaborate rejection of tau events.

The events were required to have two charged particles of momentum greater than 10 GeV/c, both identified as muons either by the muon chambers (MUB and MUF), or by the hadron calorimeter (HCAL) or by the electromagnetic calorimeters (HPC and EMF). The variable $P_{rad} = \sqrt{p_1^2 + p_2^2}/E_{beam}$, where E_{beam} is the beam energy and p_1 and p_2 are the momenta of the two muons, was required to be higher than 0.3 . There was no acollinearity cut and events with more than 5 charged particle tracks were rejected.

Because these cuts were looser than those used in the standard dimuon selection, the background from $\tau^+\tau^-$ events was higher. To reduce this background the following three criteria were introduced . When the acollinearity angle between the two muons was larger than 1°, the event was rejected if the energy deposited in the HCAL was larger than a cutoff value (see [11]). When the event had more than 2 charged particle tracks, the acollinearity angle between the two muons had to be less than 1° or both muons had to have at least one associated hit in the muon chambers. In the procedure to disentangle ISR from FSR events, a variable $|\Delta E_\gamma|$ was introduced (see 4.2). This variable was also effective in rejecting ditau events, as is shown in figure 1 which shows the distribution of ΔE_γ for simulated dimuon and ditau events after application of all cuts except the three tau rejection cuts. Events with $|\Delta E_\gamma| > 25$GeV were rejected as tau candidates.

The polar angle of the μ^- had to satisfy $20° \leq \theta_{\mu^-} \leq 160°$ for the sample used to calculate the cross sections and $11° \leq \theta_{\mu^-} \leq 169°$ for the sample used to calculate the asymmetries and the helicity cross section ratios.

After the cuts for the selection of dimuon events, and rejecting data runs where the DELPHI detector was not fully operational, the total number of dimuons in the polar angle region $11° \leq \theta_{\mu^-} \leq 169°$ amounted to 128,876, spread over 7 energy points, about 92% of these being produced at the Z^0 peak. The total number of dimuons selected in the polar angle region $20° \leq \theta_{\mu^-} \leq 160°$ was 108,865, spread over 3 energy points, about 91% of these being produced at the Z^0 peak energy.

The tau background was estimated with the simulated $\tau^+\tau^-$ events to be 0.46%.

The cosmic background was estimated from the data, by relaxing the definition of the interaction region [11] and counting the number of additional events accepted in the data sample. It was found to amount to 0.36%.

The background from two-photon events was estimated with simulated events and found to be less than 0.1% for the channel $e^+e^- \to e^+e^-\mu^+\mu^-$. For the channel $e^+e^- \to e^+e^-\tau^+\tau^-$ no events were found to satisfy the dimuon selection criteria.

From the 613K simulated $\mu^+\mu^-$ events, 513,571 remained after the dimuon selection in the polar angle region $20^\circ \leq \theta_{\mu^-} \leq 160^\circ$. These events were used for the normalisation in the cross section calculation (see 5).

4.2 Selection of $e^+e^- \to \mu^+\mu^-\gamma_{isr}$ events.

To extract the events with ISR from the dimuon sample described in section 4.1, the following variables were used:

- $p_T^{miss} = \sum_{i=1}^{N_{ch}} p_T^i$, the missing transverse momentum of the event with respect to the beam.
- α_{acol}, the acollinearity angle between the two muons
- α_{acop}, the acoplanarity angle between the production planes of the two muons with respect to the beam
- E_{em}^{neu}, the total neutral electromagnetic energy of the event. It was defined as

$$E_{em}^{neu} = E_{em}^{tot} - E_{em}^{\mu^+} - E_{em}^{\mu^-} \tag{9}$$

  with E_{em}^{tot} the total energy deposited in the electromagnetic calorimeters and $E_{em}^{\mu^+}$ ($E_{em}^{\mu^-}$) the energy deposited by the μ^+ (μ^-).

- $\Delta E_\gamma = E'_\gamma - E''_\gamma$, where

$$E'_\gamma = \sqrt{s} - E_{\mu^+} - E_{\mu^-} \tag{10}$$

  and

$$E''_\gamma = \frac{|sin(\theta_{\mu^+} + \theta_{\mu^-})|}{|sin(\theta_{\mu^+} + \theta_{\mu^-})| + sin\theta_{\mu^+} + sin\theta_{\mu^-}}\sqrt{s} \tag{11}$$

  with θ_{μ^+} and θ_{μ^-} the polar angles, and E_{μ^+} and E_{μ^-} the energies of the muons. The variable E'_γ represents the energy of the initial state photon if no final state photons are produced. The variable E''_γ is an approximation of the initial state photon energy if the muon masses are neglected and if one assumes that a single photon is emitted along the beam direction with no final state photons being produced. Figure 1 shows the distribution of ΔE_γ for simulated ISR and FSR events after applying all cuts mentioned in section 4.1.

- The isolation angle $\alpha_{\mu\gamma}$ which, for a given reconstructed photon, was taken to be the smallest of the following angles: the two angles between the muon tracks and the flightline of the photon, and the two angles between the direction opposite to

the muons and the flightline of the photon. It was assumed that the photon was produced at the vertex. The photons were reconstructed following the method described in [7]. Only photons with a reconstructed energy larger than 1 GeV were considered.

To ensure a high purity of the selected sample for all $M_{\mu\mu}$ values, the selection criteria were taken to be different in each invariant mass interval. Moreover, two sets of cuts were used depending on whether or not a photon was detected in the electromagnetic calorimeters close to one of the muons. In the barrel region the algorithm was such that when a photon was found with energy larger than 1 GeV and with isolation angle $\alpha_{\mu\gamma} < 36^\circ$ tight cuts were applied. In the end caps tight cuts were applied when a photon was found with energy higher than 1 GeV and with isolation angle $\alpha_{\mu\gamma} < 20^\circ$ or if $\alpha_{\mu\gamma} < \theta_\gamma$, with θ_γ the polar angle of the photon with respect to the beam. In all other cases loose cuts were applied. The cuts are summarised in table 1.

In the real data sample, a total of 342 ISR events were selected for the cross section calculation, after rejection of data runs in which the detector was not fully operational. These events were spread over 3 energy points, 81% of these being produced at the Z^0 peak. For the differential cross section and asymmetry calculation 399 ISR events were selected, spread over 7 energy points, 79% of these being produced at the Z^0 peak.

From the 513,697 simulated dimuons selected as described in section 4.1, 2304 ISR events were selected for the cross section calculations.

4.3 Efficiency of the selection procedure and purity of the ISR sample

The efficiency of the selection procedure and the contamination by Final State Radiation (FSR) events were studied with the sample of simulated radiative muon events with generated invariant mass $M_{\mu\mu} < 88\text{GeV/c}^2$. The events were flagged as ISR or FSR on the basis of the generator information. If initial as well as final state photons were produced, the events were labeled ISR when the generated final state photon energy was below 1 GeV and FSR otherwise. The resulting efficiency and purity are displayed as a function of the reconstructed $\mu^+\mu^-$ invariant mass in figure 2. This invariant mass was calculated using formula (13). As one can see, the purity of the sample is near 90% over the whole energy interval. The selection efficiency is about 80% at low energies and decreases to around 50% at 87 GeV.

The cosmic background was checked using the sample of ISR events selected for the cross section calculation. No additional events were found when the cuts on the interaction region definition were relaxed to $R_{imp} < 3$ cm and $|z_{imp}| < 9$ cm.

The background from $e^+e^- \to \tau^+\tau^-$ events was estimated from the sample of 270K simulated ditau events, (see section 3). No events were found to satisfy the ISR selection criteria.

The background from two-photon processes was estimated from simulated events and found to be 1.4% for the channel $e^+e^- \to e^+e^-\mu^+\mu^-$. No events in the channel $e^+e^- \to e^+e^-\tau^+\tau^-$ satisfied the ISR criteria.

5 Calculation of total cross sections

For the calculation of the cross sections, the data taken in the years 1992-1994 were used. The polar angle of the μ^- was required to be in the range $20^\circ \leq \theta_{\mu^-} \leq 160^\circ$. A total of 342 events was selected. The cross section was not calculated directly, but the ratio to the Improved Born cross section was estimated in the following way

$$\frac{\sigma_{obs}(\sqrt{s'})}{\sigma_{Born}(\sqrt{s'})} = \frac{N_{obs}(\sqrt{s'}).N_{MC}^{norm}}{N_{MC}(\sqrt{s'}).N_{obs}^{norm}} \tag{12}$$

The quantities $N_{obs}(\sqrt{s'})$ and $N_{MC}(\sqrt{s'})$ represent the number of ISR events selected as explained in 4.2, in the data and in the simulated sample, in a given $\sqrt{s'}$ interval. The quantities N_{obs}^{norm} and N_{MC}^{norm} represent the number of dimuon events selected as explained in 4.1 in the real and simulated data samples. In each $\sqrt{s'}$ interval the normalisation of the ISR sample to the full dimuon sample was calculated separately for the peak and off-peak data, after which the results were averaged. The number $N_{obs}(\sqrt{s'})$ was corrected for the two-photon background (see 4.2) and the number N_{obs}^{norm} was corrected for the background arising from cosmic and tau events (see 4.1). The other backgrounds were too small to justity a correction.

For the effective c.m. energy $\sqrt{s'}$, or equivalently the $\mu^+\mu^-$ invariant mass, the following expression was used:

$$\sqrt{s'} = M_{\mu\mu} = \sqrt{s - 2E_\gamma\sqrt{s}} \tag{13}$$

where E_γ is the photon energy, which was approximated by the quantity called E_γ'' in section 4.2. The justification for this procedure is explained in [2]. Figure 3 shows the relation between the true invariant mass and approximation (13) for simulated ISR events. The mean difference between true and reconstructed values was found to vary between 2 and 6 %.

The Improved Born cross section, $\sigma_{Born}(\sqrt{s'})$, was obtained from the DYMU3 program. The parameters used in this calculation were $M_Z = 91.25\mathrm{GeV/c^2}$, $\Gamma_Z = 2.562\mathrm{GeV/c^2}$, $\sin^2\theta_W = 0.2296$, which were the default values used by DELPHI for the generation of $\mu^+\mu^-$ events. It was shown previously [2] that the calculations made by this program and those made by the ZFITTER program [12] agreed to within 1%.

Table 2 shows the number of ISR events selected in the real and in the simulated data samples as a function of $M_{\mu\mu}$, up to an invariant mass of $87\mathrm{GeV/c^2}$. The same table shows the calculated Born cross section in the different invariant mass intervals as well as the experimental cross section obtained from formula (12). Only statistical errors were taken into account since with the present statistics the systematic errors are comparatively very small.

Figure 4 shows the ratio of the observed to Born cross sections as a function of effective c.m. energy, and the resulting experimental cross section. It also shows the cross sections for the reaction $e^+e^- \rightarrow \mu^+\mu^-(n\gamma)$ obtained near the Z^0 peak [14] after correction to Improved Born values.

6 Asymmetries and helicity cross sections.

6.1 Polar angle distributions

The data taken in the years 1991-1994 were used to obtain the distributions of the muon polar angle in the $\mu^+\mu^-$ rest frame for different $M_{\mu\mu}$ intervals. A total of 399 events were selected. The distribution of these events as a function of the $M_{\mu\mu}$ invariant mass is shown in table 3.

For events which are not produced in the e^+e^- c.m. frame, the angle between the μ^- and the e^- beam direction in the $\mu^-\mu^+$ rest frame is given by [13]:

$$\cos\theta^* = \frac{sin\frac{1}{2}(\theta_{\mu^+} - \theta_{\mu^-})}{sin\frac{1}{2}(\theta_{\mu^+} + \theta_{\mu^-})} \tag{14}$$

where θ_{μ^+} and θ_{μ^-} are the polar angles of the μ^+ and the μ^- with respect to the e^- beam in the laboratory frame. The raw distributions of $\cos\theta^*$ in the different $M_{\mu\mu}$ intervals are shown in figure 5.

In each $M_{\mu\mu}$ interval the raw $\cos\theta^*$ distribution was corrected for selection inefficiencies in the following way. It was assumed that within the limits of the present statistics forward backward asymmetries in detection efficiency could be neglected. The correction factors were therefore obtained from the folded distributions as function of $|\cos\theta^*|$, which were fitted to a function of the form

$$\frac{dN_f}{d|\cos\theta^*|} = \frac{3}{8}C(1+\cos\theta^{*2}) \tag{15}$$

in the region of $|\cos\theta^*|$ where the fit gave the smallest χ^2/N_d. The C values obtained from this fit were used to calculate correction factors in the $|\cos\theta^*|$ bins outside the fit region, namely $CF(|\cos\theta^*|) = \frac{3}{8}C(1+\cos\theta^{*2})/N_f(|\cos\theta^*|)$, where N_f is the raw number of events. In the unfolded $\cos\theta^*$ distribution, the raw bin contents for $\cos\theta^*$ equal to + and - $|\cos\theta^*|$ were corrected with the correction factors $CF(|\cos\theta^*|)$. The resulting corrected $\cos\theta^*$ distributions are also shown in figure 5 for the five $M_{\mu\mu}$ intervals considered.

The $\cos\theta^*$ distributions were then corrected for the background coming from FSR, which on average amounted to about 10%. In each $M_{\mu\mu}$ interval a distribution of the shape

$$\frac{dN}{d\cos\theta^*} = C'(\frac{3}{8}(1+\cos\theta^{*2}) + A^0_{fb}\cos\theta^*) \tag{16}$$

was subtracted, whereA^0_{fb} was the asymmetry at the Z^0 peak, which was set equal to zero. The constants C' were obtained from the integral of equation (16) which is equal to the expected number of FSR events in a given $M_{\mu\mu}$ interval. The contamination by tau events, cosmics or two-photon events was too small to justify a correction.

6.2 Forward backward asymmetries

In each $M_{\mu\mu}$ interval, the asymmetry A_{FB} was obtained by performing a maximum likelihood fit of the uncorrected $\cos\theta^*$ distribution to an expression of the form

$$\frac{dN}{dcos\theta^*} = C''[(1+cos\theta^{*2}) + \frac{8}{3}A_{FB}cos\theta^*] \tag{17}$$

Formula (17) does not include radiative corrections. Since the asymmetries determined in this analysis are Improved Born asymmetries, only the electro-weak corrections should be considered. Compared to the experimental precision they are small, and modify the asymmetry by maximum 0.02 in the energy region between 40 and 88 GeV.

The asymmetry was also calculated by counting the number of events, after correction for the selection efficiency as described in section 6.1, with positive and negative $\cos\theta^*$, since

$$A_{FB} = \frac{N_F - N_B}{N_F + N_B} \tag{18}$$

with

$$N_F = \int_0^1 \frac{dN}{dcos\theta^*} dcos\theta^* \qquad N_B = \int_{-1}^0 \frac{dN}{dcos\theta^*} dcos\theta^* \tag{19}$$

Table 3 shows the asymmetries obtained with the two methods as a function of $M_{\mu\mu}$ up to $87 GeV/c^2$.

The raw asymmetries obtained with the fit were corrected for the contamination by FSR events in a similar way as the polar angle distribution (6.1). These corrected values are also shown in table 3, and are displayed in figure 6 together with the SM prediction for the Improved Born asymmetry. Figure 6 also shows the asymmetries measured by DELPHI near the Z^0 peak (see [14]), after correction to Improved Born values. The Improved Born asymmetry was calculated with the DYMU3 program with the parameters mentioned in section 5. The only source of systematic error on the asymmetry which was considered was that resulting from the error on the purity, i.e. $\delta(A_{FB})^{fit}_{sys}$. The values of this error are shown in table 3.

6.3 Extraction of the helicity cross sections and test of the Standard Model.

From the $\cos\theta^*$ distributions corrected for selection efficiencies and for the FSR background, the cross sections $\tilde{\sigma}^{\mu}_{+}$ and $\tilde{\sigma}^{\mu}_{-}$ (see section 2.2) and their ratio were determined as follows. In each bin of the $\cos\theta^*$ distribution the corrected content was multiplied with a weight factor

$$F_{\pm} = A(1 \pm B\cos\theta^*) \tag{20}$$

where

$$A = \frac{2}{C_M(3 + C_M^2)} \qquad B = \frac{3 + C_M^2}{2C_M^2} \tag{21}$$

and $C_M = \cos\theta^*_{max}$. These weighted contents were summed for all $\cos\theta^*$ bins between -0.8 and 0.8 for the $M_{\mu\mu}$ intervals below 65 GeV, and between -0.9 and 0.9 for the other $M_{\mu\mu}$ intervals. These C_M limits were chosen to match the binning in each $M_{\mu\mu}$ interval. The statistical errors on $\tilde{\sigma}^{\mu}_{+}$ and $\tilde{\sigma}^{\mu}_{-}$ were derived from the weighted sums. For the systematic error the error on the purity of the sample was taken into account. The numbers obtained are given as a function of $M_{\mu\mu}$ in table 3. They are shown in figure 7 together with the predictions of the SM. One can conclude from this figure that within the limits of the present precision, there is no indication of any deviation from the SM.

7 Summary

Using the data collected by DELPHI until 1994, a sample of around 400 dimuon events with ISR was selected. The differential and total cross sections, and forward-backward asymmetries were determined at energies between 20 and 87 GeV. No deviation from the Standard Model was observed.

The polar angle distributions were used to determine the ratio $\frac{\sigma_{LL}+\sigma_{RR}}{\sigma_{RL}+\sigma_{LR}}$, where i(j) in σ_{ij} represents the polarisation of the incoming e^- (outgoing μ^-). The aim was to test the Standard Model near the minimum of this ratio, around 80 GeV. No evidence for new physics was seen.

8 Acknowledgements

We are greatly indebted to our technical collaborators and to the funding agencies for their support in building and operating the DELPHI detector, and to the members of the CERN-SL Division for the excellent performance of the LEP collider.

We would like to thank J.-M. Frere for suggesting the analysis in terms of helicity cross sections, and for the many fruitful discussions.

References

[1] K. Miyabayashi, *Recent electroweak results from TRISTAN*, Proceedings of the XXXth Rencontres de Moriond, Les Arcs, 1995.

[2] DELPHI collaboration, P. Abreu at al., Z. Phys. C65 (1995) 603.

[3] D. Schaile, *Precision tests of the electroweak interaction*, Proc. of the XXVIIth Int. Conf. on High Energy Physics, Glasgow, 1994, page 27.

[4] F. Berends,*Z lineshape*, in Z Physics at LEP I, CERN 89-08, Volume 1 (1989)

[5] D. Bardin et al., Nucl. Phys. B351(1991) 1

[6] J.-M. Frere, V.A. Novikov, M.I. Vysotsky, *Zeroes of the $e^+e^- \to \bar{f}f$ cross section and search for new physics*, Universite Libre de Bruxelles preprint, ULB-TH/96-5, and HEP-PH/9605241, May 95.

[7] DELPHI collaboration, P. Aarnio et al., Nucl. Instr. & Meth. A303(1991)233
P. Abreu et al., *Performance of the DELPHI detector*, CERN-PPE/95-194, submitted to Nucl. Instr. and Meth.

[8] J.E. Campagne and R. Zitoun, Z. Phys. C43(1989)469; and Proc. of the Brighton Workshop on Radiative Corrections, Sussex, July 1989.

[9] S. Jadach and Z. Was, Comp. Phys. Com. 36 (1985) 191
S. Jadach, B.F. Ward and Z. Was, Comp. Phys. Com. 66 (1991) 276

[10] J. Hilgart, R. Kleis, Comp. Phys. Com. 75 (1993) 191

[11] DELPHI collaboration, P. Abreu et al., Nucl. Phys. B417 (1994) 500
DELPHI collaboration, *Precision determination of the Z^0 parameters*, DELPHI note 95-92, PHYS 497, 30 June 1995.

[12] *ZFITTER, An Analytical Program for Fermion Pair Production in e^+e^- Annihilation*, CERN-TH. 6443/92

[13] Z. Was and S. Jadach, Phys. Rev. D41 (1990) 1425

[14] P. Abreu et al., DELPHI collaboration, Nucl. Phys. B417 (1994) 3-57
P. Abreu et al., DELPHI collaboration, Nucl. Phys. B418 (1994) 403-427
S. Almehed et al., DELPHI collaboration, DELPHI note 95-92 PHYS 497, 30 June 1995
M. Bigi et al., *DELPHI results on the Z^0 resonance parameters and measurements of fermion-pair production at LEP1.5 energies for the La Thuile and Moriond conferences 1996*, DELPHI 96-29 PHYS 603, 1996.

$M_{\mu\mu}$[GeV/c^2]	< 35	35-65	65-80	80-84	> 84
loose cuts					
p_T^{miss} [GeV/c]	-	< 5	< 4	< 4	< 3
α_{acol} [°]	> 1.5	> 1.5	> 1.5	> 1	> 1
α_{acop} [°]	< 7.5	< 7.5	< 5	< 4	< 4
E_{em}^{neu} [GeV]	-	< 2	< 2	< 2	< 2
$\lvert\Delta E_\gamma\rvert$ [GeV]	< 25	< 13.2	< 6	< 6	< 5
tight cuts					
p_T^{miss} [GeV/c]	-	< 2.5	< 1	< 1	< 1
α_{acol} [°]	> 3	> 3	> 3	> 2	> 2
α_{acop} [°]	< 5	< 5	< 4	< 3	< 3
E_{em}^{neu} [GeV]	-	< 1	< 1	< 1	< 1
$\lvert\Delta E_\gamma\rvert$ [GeV]	< 25	< 4.4	< 3	< 3	< 2.5

Table 1: Cuts applied for the selection of ISR events. The details are given in the text.

$M_{\mu\mu}$[GeV/c^2]	24-38	38-45	45-52	52-59	59-66	66-73	73-80	80-84	84-87
N_{obs}	6	11	18	10	13	23	36	61	164
N_{MC}	35	72	74	92	106	111	280	414	1120
$\sigma_{obs}/\sigma_{Born}$	0.92	0.75	1.20	0.71	0.63	1.06	0.72	0.84	0.88
	$\pm$1.33	$\pm$0.27	$\pm$0.38	$\pm$0.27	$\pm$0.21	$\pm$0.27	$\pm$0.13	$\pm$0.12	$\pm$0.07
σ^{obs} [pb]	100.	43.	51.	23.	17.	26.	21.	41.	88.
$\delta_{\sigma^{obs}}$ [pb]	144.	16.	16.	9.	6.	7.	4.	6.	7.
σ_{Born} [pb]	109.	57.	42.	33.	27.	25.	29.	48.	100.

Table 2: Number of events found in the real and simulated data sample (N_{obs} and N_{MC}) for different $M_{\mu\mu}$ intervals, ratio of measured to Born cross sections (see 5), and resulting measured cross section σ^{obs} with statistical error $\delta_{\sigma^{obs}}$. The mean Born level cross section within the energy ranges σ_{Born}, obtained from the DYMU3 program is also displayed.

$M_{\mu\mu}[\mathrm{GeV/c^2}]$	20-50	50-65	65-80	80-84	84-87
N_{FW}	20	10	12	17	55
N_{BW}	19	19	59	53	135
$A_{FB}^{counting}$ [%]	3.36±15.83	-32.6 ± 17.6	-69.5 ± 8.5	-54.0 ± 10.1	-44.2 ± 6.5
A_{FB}^{fit} unc [%]	3.28±15.82	-45.0 ± 17.7	-63.0 ± 7.4	-60.5 ± 8.9	-41.6 ± 6.4
A_{FB}^{fit} corr [%]	3.19±16.7	-48.9 ± 19.2	-70.3 ± 8.2	-66.8 ± 9.8	-46.2 ± 7.1
$\delta(A_{FB})_{sys}^{fit}$[%]	± 0.4	± 0.6	± 0.7	± 0.6	± 0.3
$\frac{\sigma_{LL}+\sigma_{RR}}{\sigma_{RL}+\sigma_{LR}}$	1.20 ± 0.46	0.24 ± 0.15	0.05 ± 0.07	0.10 ± 0.06	0.23 ± 0.06
δ_{sys}	0.051	0.012	0.006	0.006	0.005

Table 3: Observed number of events in the forward and backward hemispheres in the $\mu^+\mu^-$ c.m.s., asymmetry with statistical error calculated with the counting method and with a maximum likelihood fit, and systematic error. The fit result is given before and after correction for the FSR. Ratio $\frac{\sigma_{LL}+\sigma_{RR}}{\sigma_{RL}+\sigma_{LR}}$ (defined in section 2.2) with statistical error and systematic error δ_{sys}

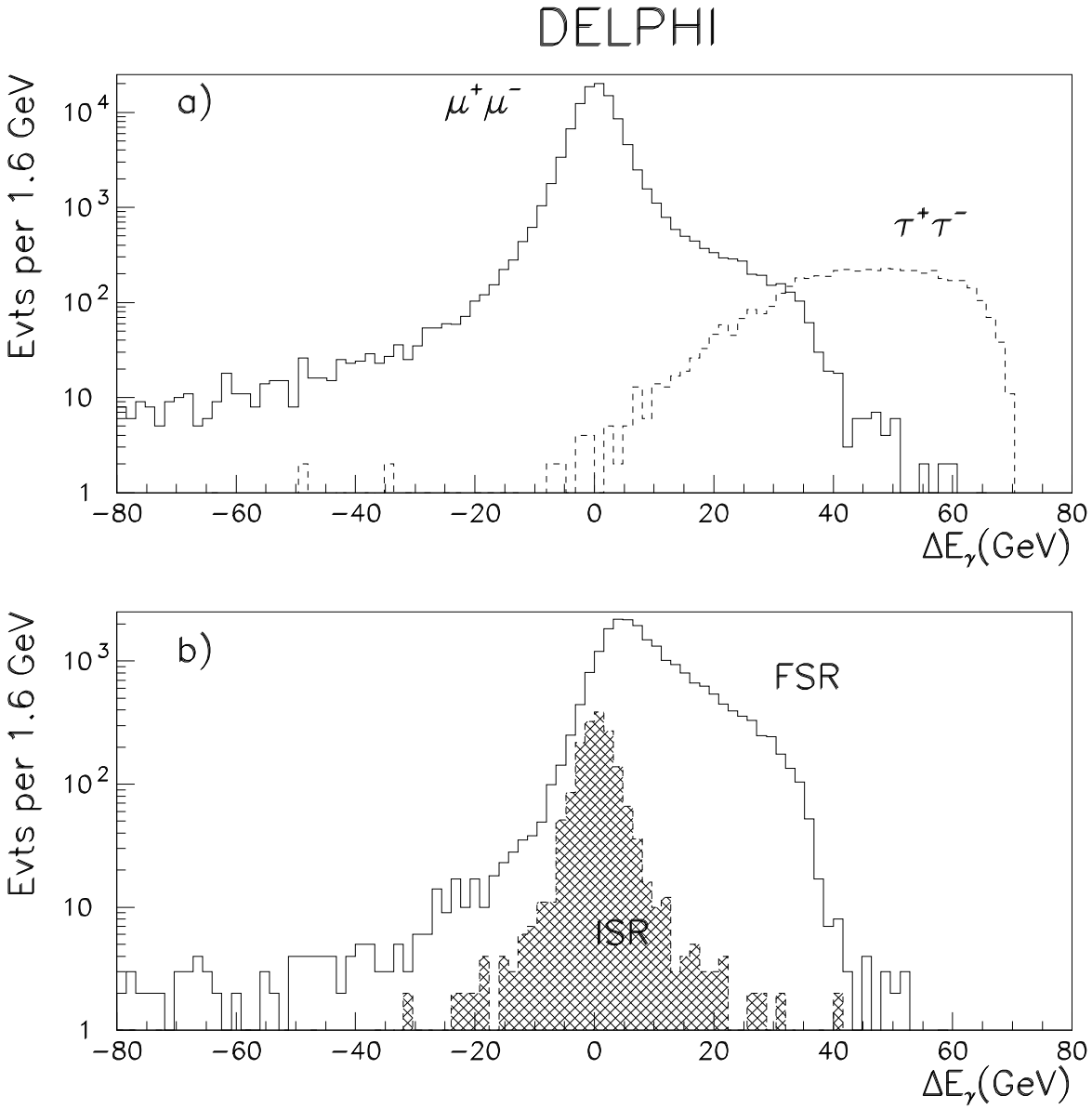

Figure 1: Distribution of ΔE_γ (see text for definition) for a) simulated dimuon events (solid line), ditau events (dashed line), after all cuts from 4 except the tau vetoes, and b) simulated ISR events (shaded area) and FSR events (solid line), after the selection procedure of section 4.

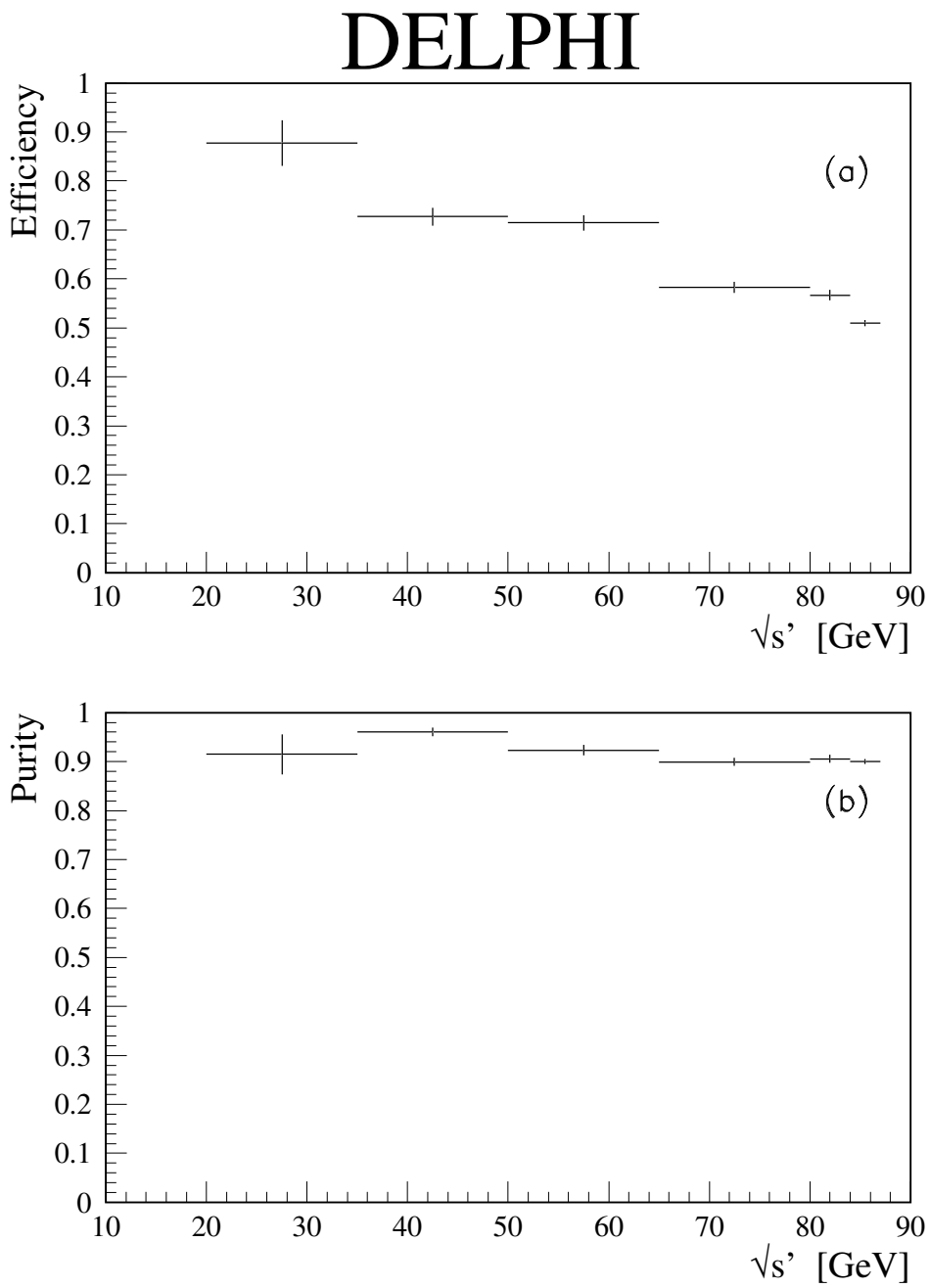

Figure 2: (a) Efficiency for the selection of ISR events and (b) purity of the sample with regard to FSR events, based on simulated radiative muon events as explained in the text.

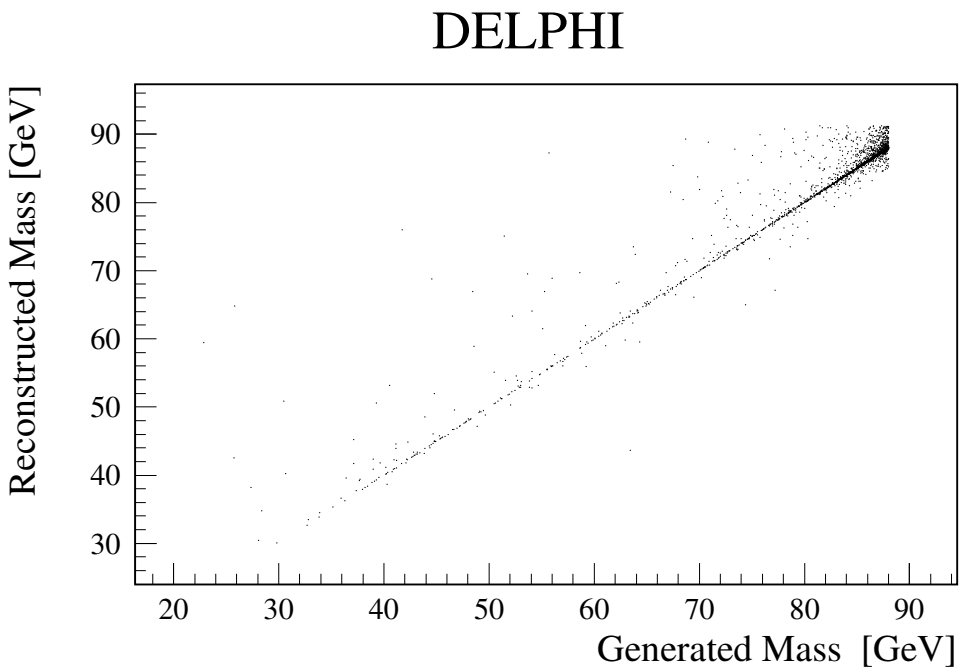

Figure 3: Reconstructed effective c.m. energy (formula 13) as function of the true $\mu^+\mu^-$ invariant mass for simulated ISR events.

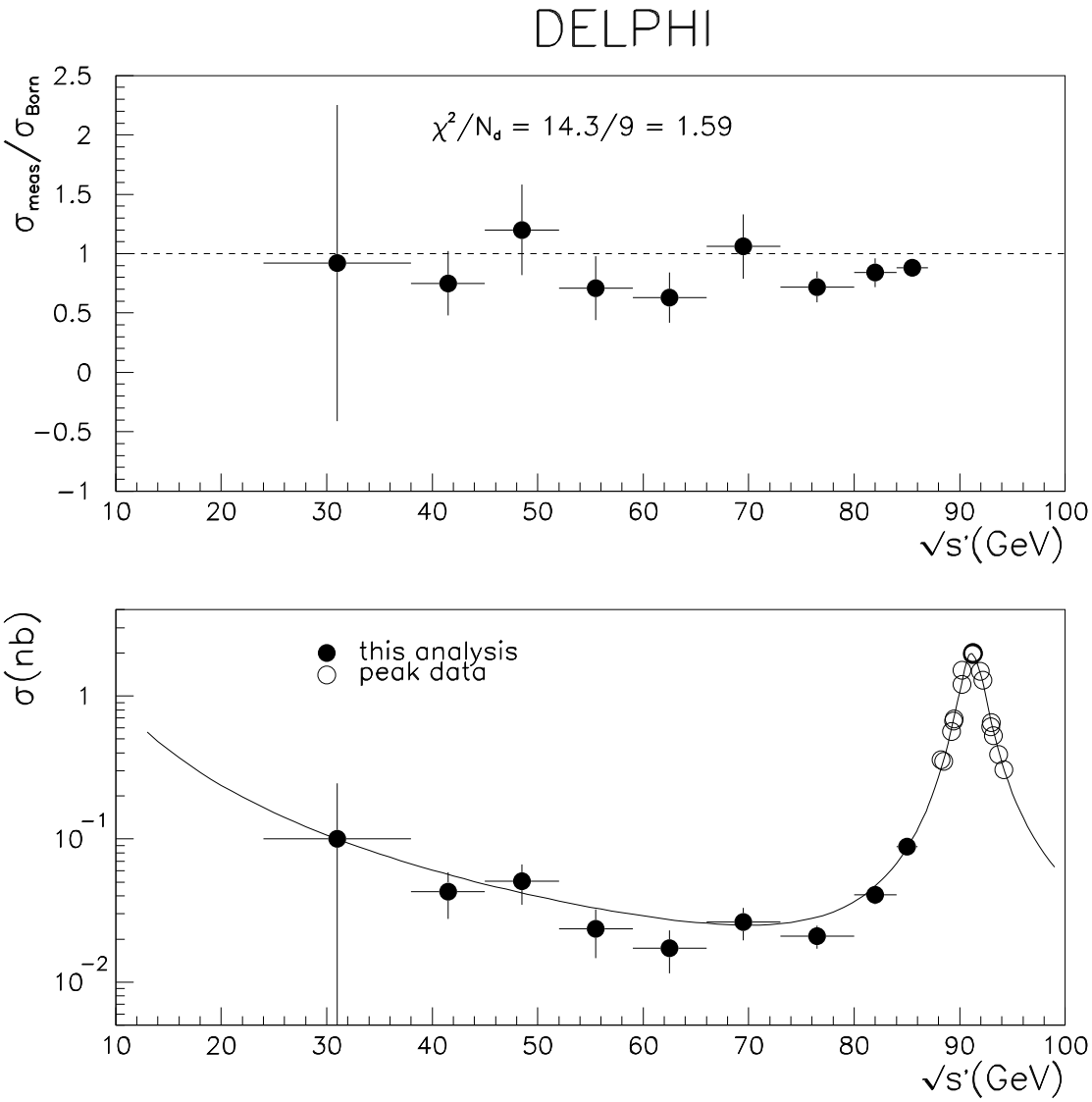

Figure 4: (a) Ratio of measured to Improved Born cross section as function of effective c.m. energy with statistical error. (b) Measured Improved Born cross section below 87 GeV (black dots) with statistical error and cross section measured at the Z^0 peak (open circles). The solid line shows the SM prediction.

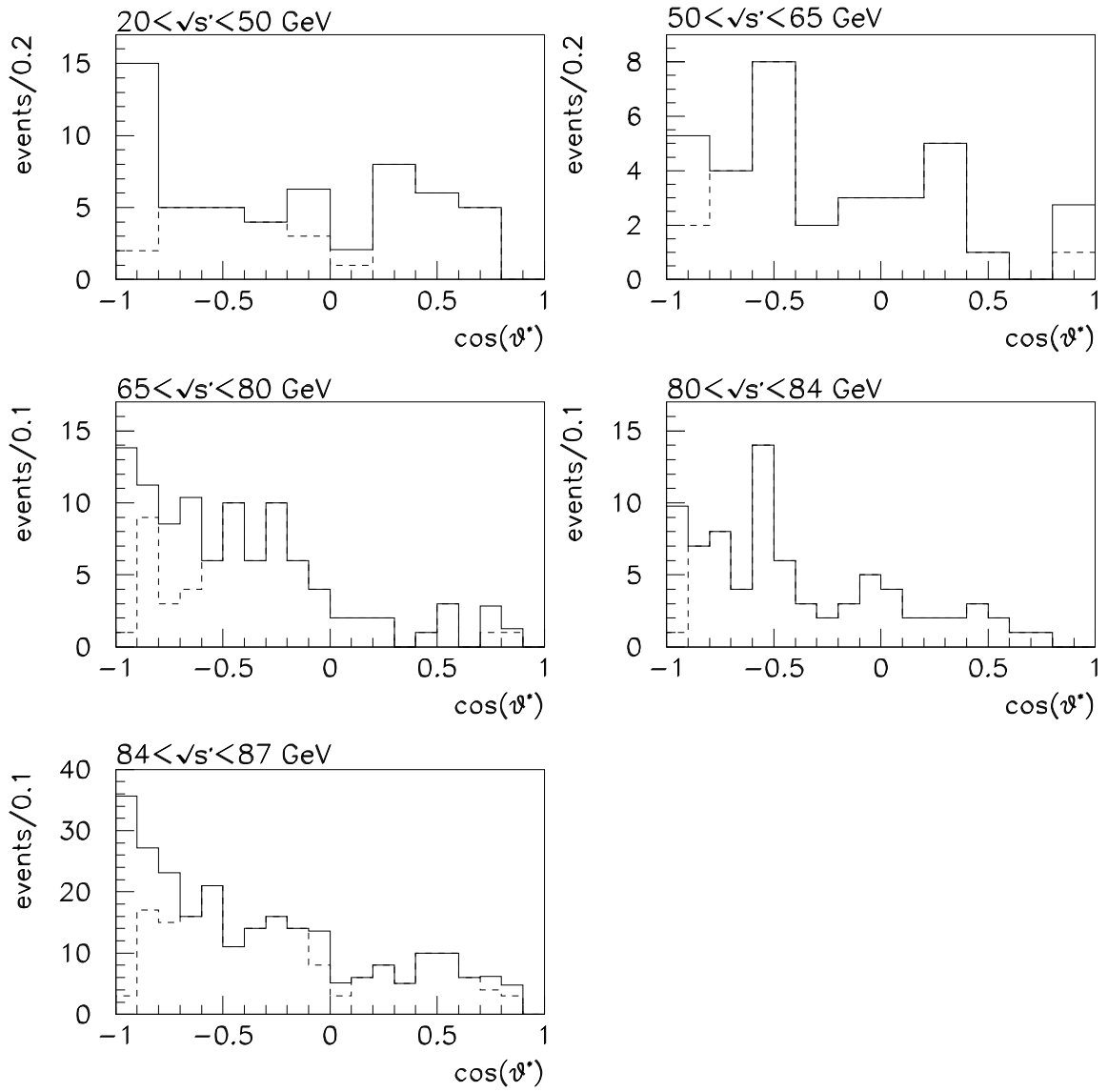

Figure 5: Distribution of $cos\theta^*$ in different effective c.m. energy intervals. The dashed line shows the raw distributions and the solid line the distributions after correction for the selection efficiency.

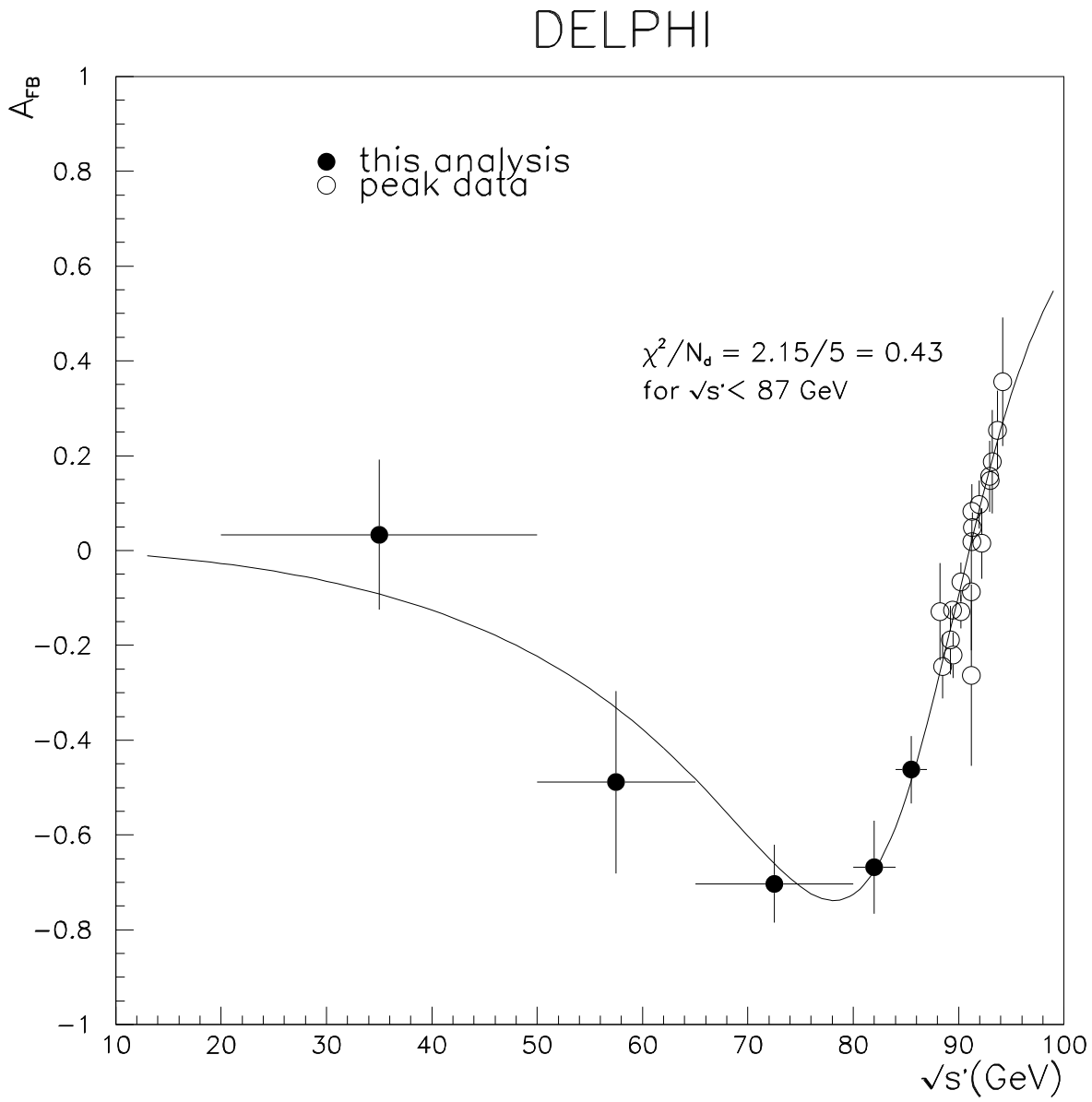

Figure 6: Improved Born asymmetry as function of effective c.m. energy. The solid line shows the SM prediction. The black points show the measurements made by DELPHI below 87 GeV, using the likelihood fit method described in the text. The errors are statistical only. The open circles show the measurements made by DELPHI at the Z^0 peak.

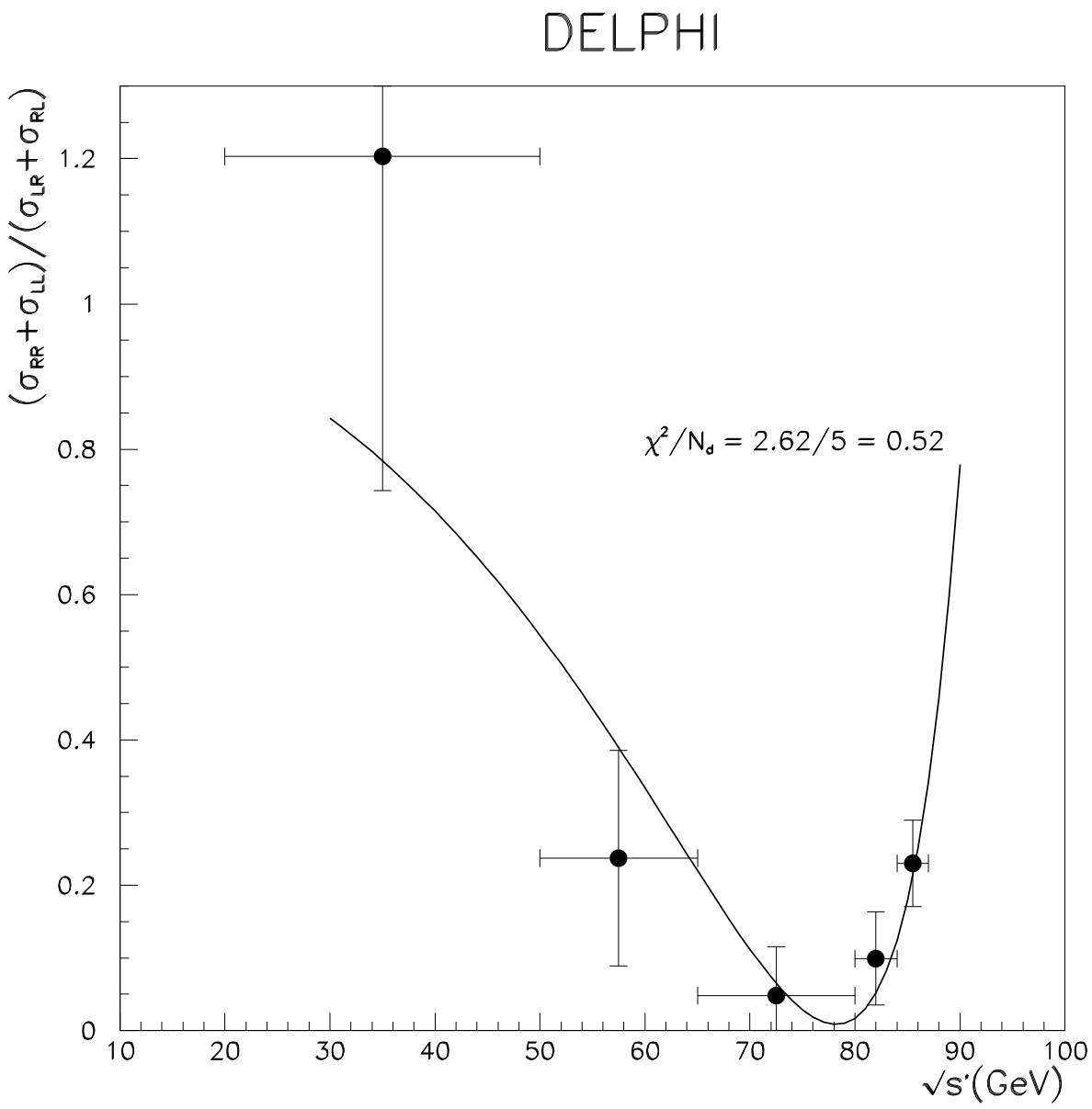

Figure 7: Ratio $\frac{\sigma_{LL}+\sigma_{RR}}{\sigma_{RL}+\sigma_{LR}}$ as function of the effective c.m. energy. The solid line shows the SM prediction.